Tactile Robot Programming: Transferring Task Constraints into Constraint-Based Unified Force-Impedance Control

Kübra Karacan, Robin Jeanne Kirschner, Hamid Sadeghian, Fan Wu, and Sami Haddadin

Abstract— Flexible manufacturing lines are required to meet the demand for customized and small batch-size products. Even though state-of-the-art tactile robots may provide the versatility for increased adaptability and flexibility, their potential is yet to be fully exploited. To support robotics deployment in manufacturing, we propose a task-based tactile robot programming paradigm that uses an object-centric tactile skill definition that directly links identified object constraints of the task to the definition of constraint-based unified force-impedance control. In this study, we first explain the basic concept of abstracting the task constraints experienced by the object and transferring them to the robot's operational space frame. Second, using the object-centric tactile skill definition, we synthesize unified force-impedance control and formalized holonomic constraints to enable flexible task execution. Later, we propose the quantified analysis metrics for the process by analyzing them as a typical example of flexible manipulation disassembly skills, e.g., levering and unscrew-driving regarding their object requirements. Supported by realistic experimental evaluation using a Franka Emika robot, our tactile robot programming approach for the direct translation between task-level constraints and robot control parameter design is shown to be a viable solution for increased robotic deployment in flexible manufacturing lines.

I. INTRODUCTION

Today's primary demand for flexible manufacturing lines is customization and, thus, small batch-size production [1]. This necessitates robots that are adaptable to changing task constraints. State-of-the-art tactile robots provide the versatility for increased adaptability and flexibility [2]. Nevertheless, their deployment for tactile and flexible interaction requires control experts. Consequently, their potentials are yet to be fully exploited [3].

One solution for increased robot deployment is to enable simple yet effective and intuitive robotic skill definitions that do not require control expertise for application. To elaborate, human experts in manufacturing sectors have comprehensive knowledge about the desired task and its requirements [4]. For instance, the task constraints, such as force and motion expected to be experienced by objects during manipulation, are well-defined. Take, for example, processing applications

Fig. 1: **Direct transfer of task information and constraints into tactile robot control for increased flexibility.** A task-oriented tactile robot programming framework translates the desired object-centric force/motion task into the robot domain.

such as milling, where the contact forces and feed speed are calculated in a standardized manner. Consequently, robots for flexible production need to be programmed to manipulate the objects, respecting those well-defined forces and motion. In the robotics community, numerous strategies for force-motion interaction have been developed, such as admittance control [5], impedance control [6], force control [7], and unified control [8], [9]. Nevertheless, robots operating under highly varying conditions, such as small batch-size sectors, lead to changing task constraints, requiring re-configuring and tuning the robot controllers accordingly.

In order to realize more natural and intuitive robot programming, it would be desired to understand the task constraints directly and feed these to the controller, see Fig. 1. Representations, e.g., the operational space framework [10], constrained-based or object-centric task specifications [11], [12], are significant steps towards this easier-to-use programming paradigm. However, directly embedding the constraints an object experiences during task execution for robot control also requires using the task constraints and directly combining them with modern controllers for flexible tactile task execution. As such, controllers can be tuned by non-experts and learned by demonstration based on analyzing the desired task constraints.

Numerous studies consider force control as a method for developing adaptive robotic skills, testing the proposed controllers with constant force values, thresholds, or constraints [13]–[17]. Nonetheless, such strategies struggle with robustness when faced with environmental uncertainties and
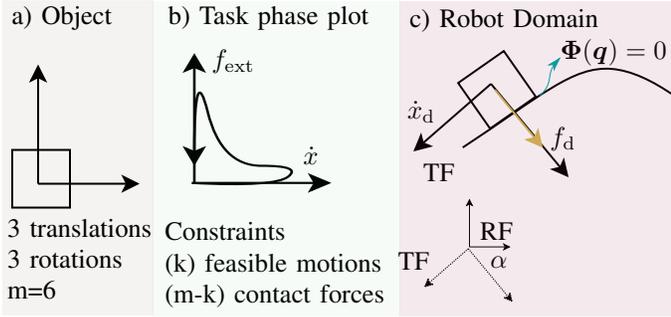
Fig. 2: **Tactile skill definition imposed by the physical task constraints.** The object's desired state dictates the task phase plot, whereas the present environment's circumstances shape it. TF: Task Frame and RF: Robot Frame.

may fail when perceptual imprecision occurs [18], [19]. Impedance control is an established method for enforcing dynamic behavior to achieve the desired motion while interacting with the environment [6]. Adaptive tuning of impedance parameters is advantageous in various applications [20], [21]. Variable impedance approaches are also used in shared autonomy applications to coordinate the motions of humans and robots and to update the predefined skill motion policy [22]. Although multiple efforts were taken among the robotic community to realize adaptive manipulation with perception uncertainties [11], [23]–[28], this is yet to be solved in principle and has not found its way into the real-world industry.

This paper proposes a task-oriented tactile robot programming paradigm that uses an object-centric tactile skill definition. This concept links identified object constraints of the task directly to the definition of constrained-based unified force-impedance control, enabling the translation between task-level constraints and robot control parameter design. For this, we

1. Introduce the basic concept of abstracting the task constraints experienced by the object and transferring them to the robot operational space frame,
2. Extend the controller schemes of our previous works [22], [29] by the formalized holonomic constraints to enable flexible task execution,
3. Analyze as a challenging, however, representative example of flexible manipulation disassembly skills starting from the respective object requirements,
4. Propose suitable process analysis metrics, and
5. Experimentally validate the approach with a Franka Emika robot.

The remainder of this paper is structured as follows. First, Sec. II formulates the processes using their required task constraints under the tactile skills and introduces the tactile robot programming method, transferring the task constraints into the robot control. The validation scenarios, the proposed task performance metrics, and the corresponding results are demonstrated and discussed in Sec. III and Sec. IV. Finally, Sec. V concludes the paper.

II. METHODOLOGY

We refer to interaction skills requiring force and motion profiles and compliant behavior as *tactile manipulation skills* [29]. Successful execution of the tactile skills is a challenging problem that involves force and form closures between the robot end-effector and the manipulation object. Every object in the real world is subject to force and motion constraints in three translational and three rotational directions, as depicted in Fig. 2a). This object-centric abstraction defines any tactile skill independent of the execution instance, like the robot. We introduced the phase plot [29] to represent the force-velocity task constraints for required skills. This representation now serves as the basis to understand the dynamic between the skill constraints based on the simple object-centric force-velocity analysis as depicted in Fig. 2b). Roughly saying, the task phase plot is the recipe for the task execution by any instance. The great challenge is formalizing this recipe so that it fits into the robot control and can handle changes in execution, which we describe in detail in the following.

A. Tactile Skill Representation

As previously mentioned, any tactile process, such as levering or unscrew-driving, is defined with specific boundary conditions in motion and force. Constraints restrict motion from a purely geometric standpoint, and the reaction force is zero along the free axis in k-dimension. In other words, during task execution, ideally, the tool moves along the free axes at velocity $\dot{\boldsymbol{x}}^{\mathrm{t}}_{\mathrm{k}\times 1}$, while the contact forces $\boldsymbol{f}^{\mathrm{t}}_{(6-\mathrm{k})\times 1}$ occur along the other axes. Selection matrices $\boldsymbol{T}_{6\times\mathrm{k}}$ and $\boldsymbol{Y}_{6\times(6-\mathrm{k})}$ are comprised of 1 and 0 to decouple the motion and force sub-spaces [7], [30]. Ideally, the task phase plot (Fig. 2b) demonstrates the entire power cycle that the object goes through, in which the force-velocity relation evolves such that the contact is established smoothly $\dot{\boldsymbol{x}} = 0$ with the surface, at the same time an external force $\boldsymbol{f}_{\mathrm{ext}} > 0$ is exerted to it.

For the exemplary scenario in Fig. 2c) the selection matrices $\boldsymbol{Y}$ and $\boldsymbol{T}$ are deduced from the physical task constraints and computed as follows. Assuming k = 5, $\boldsymbol{Y} = [\delta_i(d)]_{6\times 1}$, where a Kronecker function $\delta_i(d)$ is defined as

$$\delta_i(d) = \begin{cases} 0, & \text{if } i \neq d \\ 1, & \text{if } i = d \end{cases} \tag{1}$$

By adding zero columns to $\boldsymbol{Y}$ up to the dimension of six by six to span matrix $\boldsymbol{Y}'$, we get

$$\boldsymbol{Y}' = [\delta_{ij}(d)]_{6\times 6}, \tag{2}$$

where

$$\delta_{ij}(d) \begin{cases} 1, & \text{if } i = j = d \\ 0, & \text{else} \end{cases} \tag{3}$$

Let $\boldsymbol{T}' = \boldsymbol{I} - \boldsymbol{Y}'$ and discarding the zero columns of $\boldsymbol{T}'$ leads to $\boldsymbol{T}$. In case $d = 3$ which holds for the examples to be discussed in Sec. III, we have:

$$\boldsymbol{T} = \begin{bmatrix} 1 & 0 & 0 & 0 & 0 \\ 0 & 1 & 0 & 0 & 0 \\ 0 & 0 & 0 & 0 & 0 \\ 0 & 0 & 1 & 0 & 0 \\ 0 & 0 & 0 & 1 & 0 \\ 0 & 0 & 0 & 0 & 1 \end{bmatrix}, \boldsymbol{Y} = \begin{bmatrix} 0 \\ 0 \\ 1 \\ 0 \\ 0 \\ 0 \end{bmatrix}. \tag{4}$$
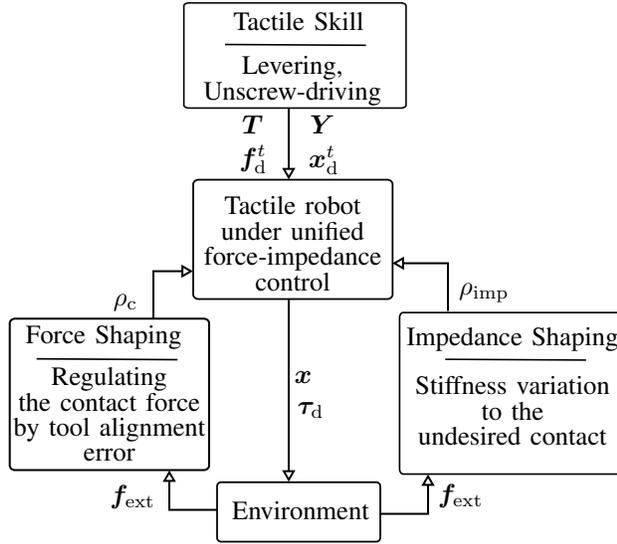
Fig. 3: **Task-oriented Tactile Robot Programming.** The controller shaping functions ensure that the controller interacts with the environment robustly and safely.

Rearranging the kinematics equation for the object using natural (geometric) and artificial constraints in the robot frame yields:

$$\dot{\boldsymbol{x}}_{6\times1} = \boldsymbol{R}_{\text{ee}}^{0}(\alpha)\boldsymbol{T}_{6\times k}\dot{\boldsymbol{x}}_{k\times1}^{\text{t}}, \ \dot{\boldsymbol{x}}_{k\times1}^{\text{t}} = \boldsymbol{T}^{\#}\boldsymbol{R}_{\text{ee}}^{0}(\alpha)^{\text{T}}\boldsymbol{J}\dot{\boldsymbol{q}}, \quad (5)$$

$$\boldsymbol{f}_{6\times1} = \boldsymbol{R}_{\text{ee}}^{0}(\alpha)\boldsymbol{Y}_{6\times(6-k)}\boldsymbol{f}_{(6-k)\times1}^{\text{t}}, \quad (6)$$

$$\boldsymbol{J}_{\text{con}} = \boldsymbol{Y}^{\#}\boldsymbol{R}_{\text{ee}}^{0}(\alpha)^{\text{T}}\boldsymbol{J}, \ \boldsymbol{J}_{\text{free}} = \boldsymbol{T}^{\#}\boldsymbol{R}_{\text{ee}}^{0}(\alpha)^{\text{T}}\boldsymbol{J}, \quad (7)$$

where $\boldsymbol{R}_{\text{ee}}^{0}(\alpha)$ is the rotation matrix of the end-effector, $\boldsymbol{J}$ is the robot Jacobian matrix. The Moore–Penrose pseudo-inverse of the matrices $\boldsymbol{Y}$ and $\boldsymbol{T}$ are:

$$\boldsymbol{T}^{\#} = (\boldsymbol{T}\boldsymbol{T}^{\text{T}})^{-1}\boldsymbol{T}, \qquad \boldsymbol{Y}^{\#} = (\boldsymbol{Y}\boldsymbol{Y}^{\text{T}})^{-1}\boldsymbol{Y}. \quad (8)$$

Continuity in the force-velocity task phase plot corresponds to the absence of abrupt power changes during the process, leading to success in the task. Therefore, we further develop the unified force-impedance control paradigm to command the object motion and force imposed by the task constraints. We also set the control shaping functions to maintain the continuity in the task phase plot by stiffness variation and force adaptation, as framed in Fig. 3.

B. Controller Design

The proposed control law for adaptive tactile skills is synthesized unified force-impedance control [8], [22] and constrained control [30], [31]. The controller has four main features:

I) following the desired motion $\boldsymbol{x}_d$ with impedance control
II) regulating the model-based contact force $\boldsymbol{\lambda}$ based on the desired force $\boldsymbol{f}_d$ without having to tune additional parameters, e.g., PID gains,
III) gravity compensation,
IV) null-space control.

The corresponding control torque $\boldsymbol{\tau}_{\text{d}} \in \mathbb{R}^n$ is defined as

$$\boldsymbol{\tau}_{\text{d}} = \boldsymbol{\tau}_{\text{imp}} + \boldsymbol{\tau}_{\text{frc}} + \boldsymbol{\tau}_{\text{g}} + \boldsymbol{\tau}_{\text{null}}, \quad (9)$$

where $\boldsymbol{\tau}_{\text{imp}}$, $\boldsymbol{\tau}_{\text{frc}}$, $\boldsymbol{\tau}_g$, and $\boldsymbol{\tau}_{\text{null}} \in \mathbb{R}^n$ are the input torque for (i) impedance control; (ii) force control; (iii) gravity compensation; and (iv) null-space control.

1) Constrained Robot Dynamics: The partially constrained robot dynamics can be deduced by an augmented Lagrangian, where the Lagrangian multiplier $\boldsymbol{\lambda}$ are the generalized contact forces when attempting to break the constraints. Using the Euler-Lagrange equations in the extended space of generalized coordinates $\boldsymbol{q} \in \mathbb{R}^n$, multiplier $\boldsymbol{\lambda} \in \mathbb{R}^{(6-k)}$, and collocated external force along the free directions $\boldsymbol{f}_{\text{free}} \in \mathbb{R}^k$ subjected to the holonomic constraints $\boldsymbol{\Phi}(\boldsymbol{q}) = \boldsymbol{0} \in \mathbb{R}^{(6-k)}$ where feasible motions are allowed in k dimensions yields

$$\boldsymbol{M}(\boldsymbol{q})\ddot{\boldsymbol{q}} + \boldsymbol{c}(\boldsymbol{q},\dot{\boldsymbol{q}}) + \boldsymbol{g}(\boldsymbol{q}) = \boldsymbol{\tau}_{\text{d}} + \boldsymbol{\tau}_{\text{ext}}, \quad (10)$$

$$\boldsymbol{\tau}_{\text{ext}} = \boldsymbol{J}_{\text{con}}^{\text{T}}(\boldsymbol{q})\boldsymbol{\lambda} + \boldsymbol{J}_{\text{free}}^{\text{T}}\boldsymbol{f}_{\text{free}}, \quad (11)$$

where $\boldsymbol{\tau}_{\text{ext}} \in \mathbb{R}^n$ represents the external torque exerted on the robot, while $\boldsymbol{M}(\boldsymbol{q})$ denotes the robot mass matrix, $\boldsymbol{c}(\boldsymbol{q},\dot{\boldsymbol{q}}) \in \mathbb{R}^n$ signifies the Coriolis and centrifugal vector, and $\boldsymbol{g}$ stands for the gravity vector in joint space. Additionally, $\boldsymbol{\tau}_{\text{d}} \in \mathbb{R}^n$ represents the control torque applied by the robot. Finally, we define the Jacobian of the constraints $\boldsymbol{J}_{\text{con}} = \frac{\partial\boldsymbol{\Phi}(\boldsymbol{q})}{\partial(\boldsymbol{q})} \in \mathbb{R}^{(6-k)\times n}$ computed in (7):

$$\dot{\boldsymbol{\Phi}}(\boldsymbol{q}) = \boldsymbol{0}_{(6-k)\times1} = \boldsymbol{J}_{\text{con}}\dot{\boldsymbol{q}}. \quad (12)$$

2) Impedance Control: The desired impedance behavior along the free axes at the tooltip is

$$\boldsymbol{f}_{\text{imp}} = \boldsymbol{K}_C\tilde{\boldsymbol{x}} + \boldsymbol{D}_C\dot{\tilde{\boldsymbol{x}}} + \boldsymbol{M}_C(\boldsymbol{q})\ddot{\boldsymbol{x}}_{\text{d}} + \boldsymbol{C}_C(\boldsymbol{q},\dot{\boldsymbol{q}})\dot{\boldsymbol{x}}_{\text{d}}, \quad (13)$$

$$\boldsymbol{\tau}_{\text{imp}} = \boldsymbol{J}_{\text{free}}^{\text{T}}\boldsymbol{f}_{\text{imp}}, \quad (14)$$

where $\boldsymbol{x} \in \mathbb{R}^k$ and $\boldsymbol{x}_{\text{d}} \in \mathbb{R}^k$ are the actual pose and the desired pose along the free axes, respectively, as well as, the pose error is $\tilde{\boldsymbol{x}} = \boldsymbol{x}_{\text{d}} - \boldsymbol{x}$. Furthermore, $\boldsymbol{K}_C$ and $\boldsymbol{D}_C \in \mathbb{R}^{k\times k}$ are diagonal stiffness and damping matrices, respectively. $\boldsymbol{M}_C(\boldsymbol{q})$ is the robot mass matrix in task space along the free axes, $\boldsymbol{C}_C(\boldsymbol{q},\dot{\boldsymbol{q}}) \in \mathbb{R}^{k\times k}$ is the Coriolis and centrifugal matrix.

The undesired contacts cause deviations from the desired pose that create either a pose error $\tilde{\boldsymbol{x}}^{\text{ee}} \in \mathbb{R}^6$, or external forces $\boldsymbol{f}_{\text{ext}}^{\text{ee}} \in \mathbb{R}^6$ at the end-effector. This phenomenon is exploited to react robustly to the undesired contacts and to re-configure the end-effector [22] by adapting the stiffness matrix $\boldsymbol{K}_C$. Having the S_{t} threshold is critical for compensating for minor environmental effects such as friction on the surface and measurement inaccuracies. It is also worth noting that using position instead of velocity or acceleration results in a less noisy signal. The normalized metric β is then coupled to $\boldsymbol{K}_C$ via ρ_{imp}.

$$\beta = 1 - \frac{\|\boldsymbol{f}_{\text{ext}}^{\text{ee}} \cdot \tilde{\boldsymbol{x}}^{\text{ee}}\|}{S_{\text{t}}}, \quad (15)$$

$$\boldsymbol{K}_C = \rho_{\text{imp}}\boldsymbol{K}_{\text{max}}, \quad (16)$$

where the stiffness adaptation parameter ρ_{imp} is calculated by

$$\dot{\rho}_{\text{imp}} = \begin{cases} \min\{\rho_{\text{r}}, 0\}, & \rho_{\text{imp}} = 1 \\ \rho_{\text{r}}, & 0 < \rho_{\text{imp}} < 1, \ \rho_{\text{imp}}(0) = 0, \\ \max\{\rho_{\text{r}}, 0\}, & \rho_{\text{imp}} = 0 \end{cases}$$

$$\quad (17)$$

and ρ_{r} is

$$\rho_{\text{r}} = \beta\rho_{\text{imp}} + \rho_{\text{min}}. \quad (18)$$
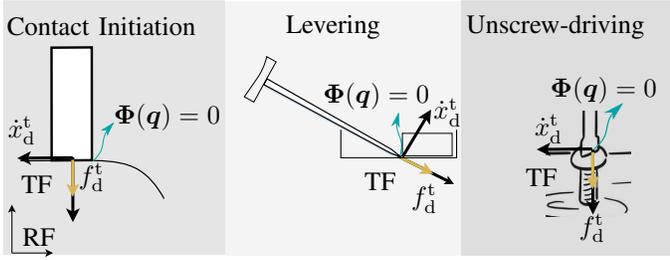
Fig. 4: **Tactile disassembly skill examples.** Task constraints $\boldsymbol{T}$ and $\boldsymbol{Y}$ encode the motion and force sub-spaces and are the same in the shown cases.

Once the robot's behavior is compliant $\rho_{\text{imp}} = 0$, it reacts to the environment. Adapted to the current environmental conditions, the robot recovers its maximum stiffness and resumes the desired motion from its present configuration. It should be noted that a slight positive constant $\rho_{\min}$ is included in the shaping function dynamics to provide an initial increment for the situation $\rho_{\text{imp}} = 0$.

3) Force Control: Instead of having to tune gains and parameters to specific situations, we chose to design the force controller $\boldsymbol{f}_{\text{frc}}$ to be the difference between the desired $\boldsymbol{f}_{\text{d}} \in \mathbb{R}^{(6-k)}$ and the model-based contact force $\boldsymbol{\lambda}$, considering $\boldsymbol{\lambda}$ should be equal to $\boldsymbol{f}_{\text{d}}$ [30]

$$\boldsymbol{f}_{\text{frc}} = \boldsymbol{f}_{\text{d}} - \boldsymbol{\lambda} \,. \tag{19}$$

To calculate the model-based contact force $\boldsymbol{\lambda}$, the kinematics equation at acceleration level in (20) is sol it.

$$\ddot{\boldsymbol{\Phi}}(\boldsymbol{q}) = \boldsymbol{0}_{(6-\text{k})\times 1} = \dot{\boldsymbol{J}}_{\text{con}}\dot{\boldsymbol{q}} + \boldsymbol{J}_{\text{con}}\ddot{\boldsymbol{q}} \tag{20}$$

After inserting the joint accelerations from (10) and the input torque (9), rearranging the terms yields

$$\begin{aligned}
\boldsymbol{\lambda} = &-\boldsymbol{J}_{\text{con}}^{\#}\boldsymbol{J}_{\text{con}}\boldsymbol{M}^{-1}(\boldsymbol{J}_{\text{free}}^{\text{T}}\boldsymbol{f}_{\text{imp}} + \boldsymbol{\tau}_{\text{null}}) + \\
&\boldsymbol{J}_{\text{con}}^{\#}\boldsymbol{J}_{\text{con}}\boldsymbol{M}^{-1}\boldsymbol{c} - \boldsymbol{J}_{\text{con}}^{\#}\dot{\boldsymbol{J}}_{\text{con}}\dot{\boldsymbol{q}} + \\
&\boldsymbol{J}_{\text{con}}^{\#}\boldsymbol{J}_{\text{con}}\boldsymbol{M}^{-1}(\boldsymbol{J}_{\text{free}}^{\text{T}}\boldsymbol{f}_{\text{free}}) \,.
\end{aligned} \tag{21}$$

The inertia-weighted pseudo-inverse of the constraint Jacobian $\boldsymbol{J}_{\text{con}}$ is $\boldsymbol{J}_{\text{con}}^{\#} = (\boldsymbol{J}_{\text{con}}\boldsymbol{M}^{-1}\boldsymbol{J}_{\text{con}}^{\text{T}})^{-1}$. Finally, the input torque to control the desired contact force is

$$\boldsymbol{\tau}_{\text{frc}} = \rho_{\text{frc}}\boldsymbol{J}_{\text{con}}^{\text{T}}\boldsymbol{f}_{\text{frc}} \,. \tag{22}$$

Additionally, we design the force shaping function ρ_{frc}. The force shaping function combines ρ_{c} and ρ_{imp} to adapt the commanded force caused by the tool alignment error and undesired contacts.

$$\rho_{\text{frc}} = \rho_{\text{imp}}\rho_{\text{c}} \,. \tag{23}$$

The robot tolerates the tool alignment error $\|\boldsymbol{f}_{\text{d}}^{\text{ee}} \cdot \tilde{\boldsymbol{x}}^{\text{ee}}\|$ during the contact by the lower limit of $S_{\min}$ within $\delta_{\text{c}} > 0$. Moreover, if the robot loses surface contact due to the large tool alignment error, the robot is only impedance-controlled and follows the desired motion.

$$\rho_{\text{c}} = \begin{cases} 1 \,, & \|\boldsymbol{f}_{\text{d}}^{\text{ee}} \cdot \tilde{\boldsymbol{x}}^{\text{ee}}\| \leq S_{\min} \\ 0.5(1 + \cos((\pi \frac{\|\boldsymbol{f}_{\text{d}}^{\text{ee}} \cdot \tilde{\boldsymbol{x}}^{\text{ee}}\| - S_{\min}}{\delta_{\text{c}}}))) \,, & S_{\min} < \|\boldsymbol{f}_{\text{d}}^{\text{ee}} \cdot \tilde{\boldsymbol{x}}^{\text{ee}}\| \\ & \leq S_{\min} + \delta_{\text{c}} \\ 0 \,, & \text{otherwise.} \end{cases} \tag{24}$$

It is noteworthy to mention that even though the robot behaves compliantly to the undesired contacts with the help of the control shaping functions as well as we fully decouple the motion and force sub-spaces, using $\boldsymbol{T}$ and $\boldsymbol{Y}$ based on the task constraints, the unification of force and impedance control, as well as, variable stiffness in the impedance controller may compromise the stability [32]. However, one may guarantee stability by installing virtual energy tanks [33].

Next, the validation scenarios and relevant evaluation metrics for the exemplary tactile skills are discussed.

III. VALIDATION SCENARIOS

We focus on the tasks from the disassembly processes as our representative examples. Levering and unscrew-driving are two crucial skills widely used in disassembly tasks involved in electronics waste recycling, a field heavily dependent on manual labor and challenging to automate by using robots [34].

A. Levering

The levering operation is one of the main steps in the disassembly pipeline. For instance, when removing the PCB from a heat-cost-allocator (HCA), levering lets us apply moments using the levering support at the edge of the HCA, as shown in Fig. 4. One approach to levering is to use periodic motions $\boldsymbol{x}_d^t$ while maintaining contact $\boldsymbol{f}_d^t$ perpendicular to the tooltip, essentially when the desired force is complicated to define to lever an object [34]. Levering is likely successful when the locking mechanism is broken or fully opened, thereby stuck. In other words, it is difficult to define a goal for a successful execution.

We design an experimental setup to enable reproducible comparisons by choosing a car outlet socket as our exemplary object and manufacturing an aluminum counterpart to fix it firmly. The lid of a car socket outlet is levered by using the peg. The length and diameter of the peg are $20\,\text{mm}$ and $3\,\text{mm}$, respectively. The experiment starts with no contact, and the algorithm is defined such that the robot should start with force control to establish contact. The expected behavior is that if no contact is sensed, the robot should stop force control and restart when contact is sensed. The motion is a function of time t, whereas amplitude and frequency are $B = 0.04\,\text{m}$ and $\omega = 0.15\,\text{Hz}$, respectively.

$$\boldsymbol{x}_d^t = [0\,|\,B\sin(2\pi\omega t)|\,0\,0\,0]^T \,, \boldsymbol{f}_d^t = [12] \,, \tag{25}$$
$$S_t = 0.5 \,, S_{\min} = 0.0001 \,, \delta_c = 0.7 \,. \tag{26}$$

The task constraints $\boldsymbol{T}$ and $\boldsymbol{Y}$ are the same as derived in (4).

B. Unscrew-driving

Electronic unscrew-driving is possible in two ways: button-triggered or push-to-start. As button-triggered screwdriver requires additional setups [35], we analyze the push-to-start electronic screwdriver-based process. The process requires the screwdriver to be pushed while the screw moves in the opposite direction. Push-to-start is generally triggered by a certain amount of force, as provided in the tool's datasheet. The tool should also be perpendicular to the screw to maintain contact. During our experiments, we use an M8x25mm screw and drill the thread through an aluminum
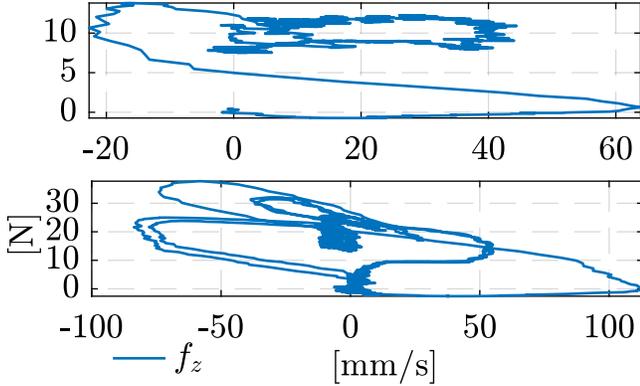
Fig. 5: **Task phase plots.** Task evolution is presented for Top: levering and Bottom: unscrew-driving. Continuity in the plots shows the robustness to varying external forces, thereby, the successful execution of the process.

Fig. 6: **Norm of the linear and rotational velocities of the end effector.** Top: Levering and Bottom: unscrew-driving. Constant orientation due to rotational velocity around zero while moving means that the robot maintains contact.

counterpart to fix it in our experimental setup. While the same task constraints T and Y are used, the rest of the parameters are as follows:

$$\boldsymbol{x}_d^t = [0\,0\,0\,0\,0]^T \,,\, \boldsymbol{f}_d^t = [20] \,, \tag{27}$$
$$S_t = 3.5 \,,\, S_{\min} = 0.0001 \,,\, \delta_c = 1.8 \,. \tag{28}$$

The translational $\boldsymbol{K}_{\mathrm{max,t}}$ and rotational $\boldsymbol{K}_{\mathrm{max,r}}$ stiffness used in the experiments are $1500\,\mathrm{N/m}$ and $200\,\mathrm{Nm/rad}$, respectively, whereas the damping ratio is $\mathrm{diag}[0.7, 0.7, 0.7, 1, 1, 1]$.

C. Remarks

Based on the levering and unscrew-driving process definitions, for successfully executing the process, the robot should be i) positioning the tool as accurately as possible at a desired region of interest, ii) applying a force profile as accurately as possible, iii) ensuring an accurate motion and process success even if undesired external forces occur, iv) deviating from a defined motion profile as little as possible. Thus, our task-oriented tactile robot programming framework is evaluated for these four items under the categories of a) position accuracy, b) displacement tolerance, c) force tolerance, and d) force and motion error. A Franka Emika robot is used for the experiments, and the robot's internal sensing capabilities are used to measure the position, velocity, and external force/torque at the end-effector [36].

IV. RESULTS AND DISCUSSION

For the levering scenario, the expected behavior for the robot is to move to the contact and maintain the contact force of $12\,\mathrm{N}$ with the lid in the z-direction while moving along the x-direction in the end-effector frame. In contrast, the lid is levered about the y-direction. As the robot is compliant in the z-direction, it moves with the lid along the z-direction due to force control while moving along the x-direction due to impedance control. In this case, the motion in the z-direction is treated as a tool alignment error and regulated by the force control shaping function ρ_c. Thus, the robot can only move within the threshold δ_c, meaning that the force is reduced to zero after a certain distance by ρ_{frc}. During unscrew-driving, the robot pushes the screw with the force of $20\,\mathrm{N}$ in the
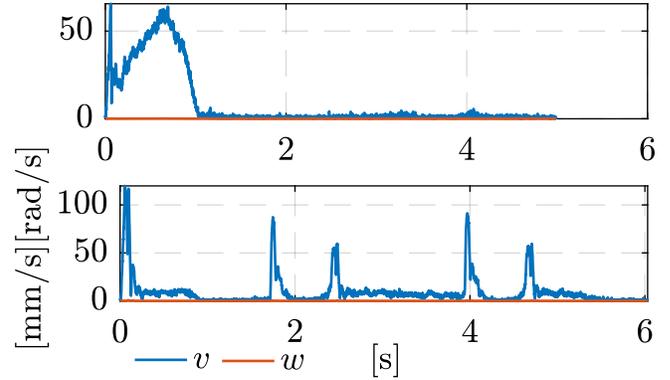
z-direction while moving in the opposite direction. As the screw gets loose during the process, it starts moving in other directions, altering the external force at the end-effector. Therefore, the stiffness adaptation ρ_{imp} is activated, and due to this compliant behavior, the robot's end-effector is pushed by the external force and reconfigured itself. This process continues until the screw is fully unscrewed to $25\,\mathrm{mm}$.

The task phase plot is developed with the external force and velocity in the z-direction in the robot's task space. The force and velocity evolution also translates to the power development during the task, as shown in Fig. 5. Therefore, the continuity in the plot means the task proceeds successfully. In particular, the levering process starts with no-contact $0\,\mathrm{N}$. The initial back and forth motion around $60\,\mathrm{mm/s}$ and $-20\,\mathrm{mm/s}$ with around $15\,\mathrm{N}$ is the initial contact. After the initial contact with the lid, the force decreases to $12\,\mathrm{N}$ while it moves together with the lid with $40\,\mathrm{mm/s}$. Later, the contact force is maintained around $7\,\mathrm{N}$ at $0\,\mathrm{mm/s}$, where the lid is fully opened and cannot move anymore. During the unscrew-driving process, after the initial contact of $30\,\mathrm{N}$, the robot starts unscrew-driving by the force of $20\,\mathrm{N}$. As it can be seen in the plot in Fig. 5, while the robot applies the force of $20\,\mathrm{N}$, it also moves up to the velocity of $-50\,\mathrm{mm/s}$, as the screw keeps unscrewed. However, later, the robot stops moving and applying force. After adapting to the current configuration, the robot keeps repeating the pattern in the task phase plot. The continuity in the plot during levering and unscrew-driving can be interpreted as a successful task. Additionally, it shows robustness to varying external forces.

The position accuracy of aligning the tool requires constant end-effector orientation during the processes, which is crucial to establishing and maintaining contact. The norm of the angular velocity w.r.t the end effector in Fig. 6 is $\approx 0\,\mathrm{rad/s}$ both in levering and unscrew-driving, which shows us the robot maintains the contact robustly during the process.

Force-motion profile errors can be analyzed in the force and position plots, as shown in Fig. 7 and Fig. 8. Notably, the commanded force to the robot is the desired force times ρ_{frc}. For instance, as shown in Fig. 7, ρ_{frc} decrease to app. 0.6, such that the commanded force $\boldsymbol{f}_z$ reduced from $12\,\mathrm{N}$ to app.
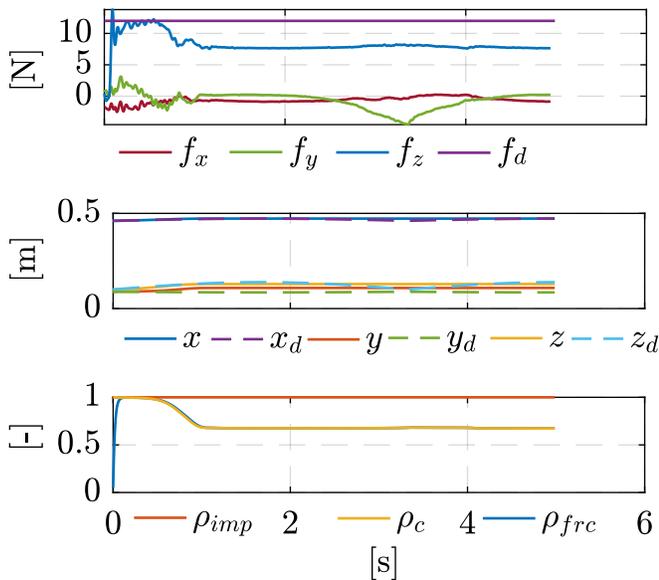
Fig. 7: **Performance metrics results for levering.** Top: desired vs. measured force in the end effector frame, Middle: desired vs. actual motion in the base frame, and Bottom: controller shaping functions.

7.2 N. While tracking the motion and forces as accurately as possible is important, for successful execution, levering and unscrew-driving are the processes that need to tolerate the force and displacement imperfections due to, e.g., a loose screw moving in the thread. Here, we can comment that our tactile robot programming framework allows, yet limits the force and displacement tolerances by the control shaping functions such that they regulate the stiffness and commanded forces for the certain thresholds $S_t, S_{\min}$, and δ_c that the human experts set beforehand to allow acceptable deviations while ensuring successful executions.

In general, the focus in tactile skills relies on contact/tool alignment ρ_c and compliant behavior ρ_{imp}, namely, force and displacement tolerance, such that after specific tool alignment error, the robot should stop applying force or if the impedance shaping is activated due to the motion error and external forces occurred. Specifically, the levering process is analyzed and based on the results in Fig. 7, the contact/tool alignment during sinusoidal motion or force-displacement tolerance is crucial to achieving a robust levering process as the lid moves primarily, and the robot should maintain contact between the tool and the lid during the motion.

In addition, unscrew-driving demands compliant behavior or displacement tolerance, as can be interpreted from the results in Fig. 8. It is also predictable as the robot should allow the screw to move upwards while pushing it to trigger the screwdriver, and this requires the screwdriver to be perpendicular to the screw to maintain contact. The impedance shaping is activated if the contact is about to be broken, leading to external force and motion error. Here, the robot stops force control while compliant due to decreasing ρ_{imp}. The stiffness is fully recovered in the current configuration, and the robot re-starts applying force after correct tool alignment. The authors would like to mention that further study should focus on deciding $S_t, \rho_{\min}$, and δ_c instead of fine-tuning the current surface material properties, such as friction and rigidity.
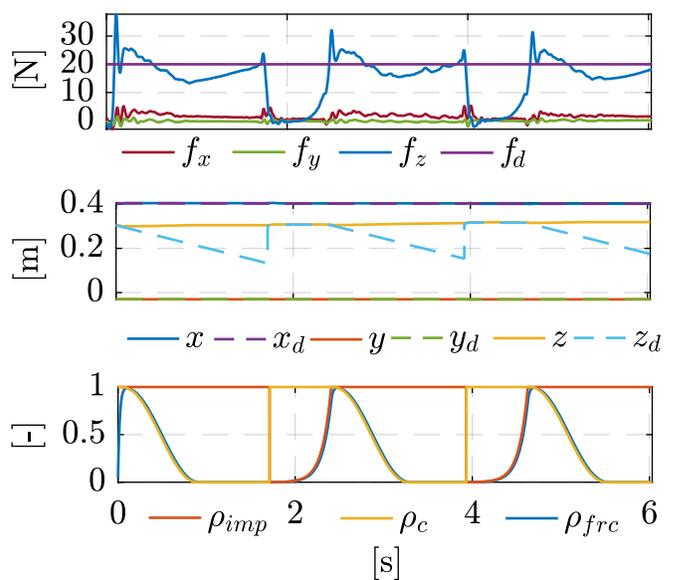
Fig. 8: **Performance metrics results for unscrew-driving.** Top: desired vs. measured force in the end effector frame, Middle: desired vs. actual motion in the base frame, and Bottom: controller shaping functions.

V. Conclusion

Cutting-edge tactile robots offer improved adaptability and flexibility, but still, their programming using force- or impedance control is relatively static and requires expert knowledge. Reaching the full potential of flexible manipulation task execution in real-world scenarios requires highly simplified programming for non-experts. Thus, we propose a task-oriented tactile robot programming framework to successfully deploy tactile robotics in manufacturing that exploits object-centric tactile skill definition.

The core concept consists of a) the basic knowledge of the forces and motion constraints a real-world object is subject to; b) using a force-velocity representation called task phase showing the change of these constraints during the task; and c) transferring this intuitive representation into the robot control, without requiring the robot operators expert knowledge about controller parameterization. We apply this scheme to establish constraint-based unified force-impedance control for common manipulation skills, which we validate in real-life experiments using the tasks of unscrew-driving and levering with a Franka Emika robot manipulator by evaluating in terms of the proposed analysis metrics i) position accuracy, ii) displacement tolerance, iii) force tolerance, and iv) force and motion error. Finally, our approach to simplify tactile robot programming and enable the direct translation between task-level constraints and robot control is a potential solution for increased robotic deployment in flexible manufacturing lines.

Future work will focus on blending the tactile disassembly skills by extending our task-oriented tactile robot programming approach.

References

[1] E. C. Balta, K. Jain, Y. Lin, D. Tilbury, K. Barton, and Z. M. Mao, "Production as a service: A centralized framework for small batch manufacturing," in *2017 13th IEEE Conference on Automation Science and Engineering (CASE)*, 2017, pp. 382–389.

[2] S. Haddadin, L. Johannsmeier, and F. Díaz Ledezma, "Tactile robots as a central embodiment of the tactile internet," in *Proceedings of the IEEE*, vol. 107, no. 2, Feb. 2019, pp. 471–487.

[3] A. Billard and D. Kragic, "Trends and challenges in robot manipulation," *Science*, vol. 364, no. 6446, p. eaat8414, 2019. [Online]. Available: https://www.science.org/doi/abs/10.1126/science.aat8414

[4] A. Lambert and S. Gupta, "Disassembly modeling for assembly, maintenance, reuse and recycling," 12 2004.

[5] W. S. Newman, "Stability and Performance Limits of Interaction Controllers," *Journal of Dynamic Systems, Measurement, and Control*, vol. 114, no. 4, pp. 563–570, Dec. 1992, _eprint: https://asmedigitalcollection.asme.org/dynamicsystems/article-pdf/114/4/563/5551865/563_1.pdf. [Online]. Available: https://doi.org/10.1115/1.2897725

[6] N. Hogan, "Impedance control: An approach to manipulation," in *1984 American Control Conference*, 1984, pp. 304–313.

[7] O. Khatib, "A unified approach for motion and force control of robot manipulators: The operational space formulation," *IEEE J. Robotics Autom.*, vol. 3, pp. 43–53, 1987.

[8] C. Schindlbeck and S. Haddadin, "Unified Passivity-Based Cartesian Force / Impedance Control for Rigid and Flexible Joint Robots via Task-Energy Tanks," *2015 IEEE International Conference on Robotics and Automation (ICRA)*, pp. 440–447, 2015.

[9] M. Iskandar, C. Ott, A. Albu-Schäffer, B. Siciliano, and A. Dietrich, "Hybrid force-impedance control for fast end-effector motions," *IEEE Robotics and Automation Letters*, vol. 8, no. 7, pp. 3931–3938, July 2023.

[10] O. Khatib, "Inertial properties in robotic manipulation: An object-level framework," *The International Journal of Robotics Research*, vol. 14, no. 1, pp. 19–36, 1995. [Online]. Available: https://doi.org/10.1177/027836499501400103

[11] J. D. Schutter, T. D. Laet, J. Rutgeerts, W. Decré, R. Smits, E. Aertbeliën, K. Claes, and H. Bruyninckx, "Constraint-based task specification and estimation for sensor-based robot systems in the presence of geometric uncertainty," *The International Journal of Robotics Research*, vol. 26, no. 5, pp. 433–455, 2007. [Online]. Available: https://doi.org/10.1177/0278364907078091107

[12] T. Migimatsu and J. Bohg, "Object-centric task and motion planning in dynamic environments," *IEEE Robotics and Automation Letters*, vol. 5, no. 2, pp. 844–851, 2020.

[13] A. Cherubini, R. Passama, A. Crosnier, A. Lasnier, and P. Fraisse, "Collaborative manufacturing with physical human–robot interaction," *Robotics and Computer-Integrated Manufacturing*, vol. 40, pp. 1–13, 2016. [Online]. Available: https://www.sciencedirect.com/science/article/pii/S0736584515301769

[14] F. Ficuciello, L. Villani, and B. Siciliano, "Variable impedance control of redundant manipulators for intuitive human–robot physical interaction," *IEEE Transactions on Robotics*, vol. 31, no. 4, pp. 850–863, Aug 2015.

[15] W. He, Y. Chen, and Z. Yin, "Adaptive neural network control of an uncertain robot with full-state constraints," *IEEE Transactions on Cybernetics*, vol. 46, no. 3, pp. 620–629, March 2016.

[16] F. Kulakov, G. V. Alferov, P. Efimova, S. Chernakova, and D. Shymanchuk, "Modeling and control of robot manipulators with the constraints at the moving objects," in *2015 International Conference "Stability and Control Processes" in Memory of V.I. Zubov (SCP)*, Oct 2015, pp. 102–105.

[17] C. Ott, A. Dietrich, and A. Albu-Schäffer, "Prioritized multi-task compliance control of redundant manipulators," *Automatica*, vol. 53, pp. 416–423, 2015. [Online]. Available: https://www.sciencedirect.com/science/article/pii/S0005109815000163

[18] P. Pastor, M. Kalakrishnan, L. Righetti, and S. Schaal, "Towards associative skill memories," in *2012 12th IEEE-RAS International Conference on Humanoid Robots (Humanoids 2012)*, Nov 2012, pp. 309–315.

[19] A. Kramberger, A. Gams, B. Nemec, C. Schou, D. Chrysostomou, O. Madsen, and A. Ude, "Transfer of contact skills to new environ-mental conditions," in *2016 IEEE-RAS 16th International Conference on Humanoid Robots (Humanoids)*, 2016, pp. 668–675.

[20] C. Yang, G. Ganesh, S. Haddadin, S. Parusel, A. Albu-Schaeffer, and E. Burdet, "Human-like adaptation of force and impedance in stable and unstable interactions," *IEEE transactions on robotics*, vol. 27, no. 5, pp. 918–930, 2011.

[21] F. J. Abu-Dakka and M. Saveriano, "Variable impedance control and learning—a review," *Frontiers in Robotics and AI*, vol. 7, 2020. [Online]. Available: https://www.frontiersin.org/articles/10.3389/frobt.2020.590681

[22] K. Karacan, H. Sadeghian, R. Kirschner, and S. Haddadin, "Passivity-based skill motion learning in stiffness-adaptive unified force-impedance control," in *2022 IEEE/RSJ International Conference on Intelligent Robots and Systems (IROS)*, 2022, pp. 9604–9611.

[23] P. Pastor, M. Kalakrishnan, S. Chitta, E. Theodorou, and S. Schaal, "Skill learning and task outcome prediction for manipulation," in *2011 IEEE International Conference on Robotics and Automation*, May 2011, pp. 3828–3834.

[24] F. Ruggiero, V. Lippiello, and B. Siciliano, "Nonprehensile dynamic manipulation: A survey," *IEEE Robotics and Automation Letters*, vol. 3, no. 3, pp. 1711–1718, 2018.

[25] M. Suomalainen, Y. Karayiannidis, and V. Kyrki, "A survey of robot manipulation in contact," *Robotics and Autonomous Systems*, vol. 156, p. 104224, 2022. [Online]. Available: https://www.sciencedirect.com/science/article/pii/S0921889022001312

[26] M. Qin, J. Brawer, and B. Scassellati, "Robot tool use: A survey," *Frontiers in Robotics and AI*, vol. 9, 2023. [Online]. Available: https://www.frontiersin.org/articles/10.3389/frobt.2022.1009488

[27] European Union, 1994-2023, "Self-reconfiguration of a robotic work-cell for the recycling of electronic waste," https://cordis.europa.eu/project/id/871352/reporting/de, Last accessed on 2023-06-15.

[28] K. Karacan, D. Grover, H. Sadeghian, F. Wu, and S. Haddadin, "Tactile exploration using unified force-impedance control," Jul 2023, p. under publication, 22nd IFAC World Congress.

[29] K. Karacan, R. J. Kirschner, H. Sadeghian, F. Wu, and S. Haddadin, "The inherent representation of tactile manipulation using unified force-impedance control," December 2023, p. under publication, 2023 IEEE 62nd Conference on Decision and Control (CDC).

[30] A. De Luca and C. Manes, "Modeling of robots in contact with a dynamic environment," *IEEE Transactions on Robotics and Automation*, vol. 10, no. 4, pp. 542–548, Aug 1994.

[31] B. Siciliano, L. Sciavicco, L. Villani, and G. Oriolo, *Robotics: Modelling, Planning and Control*, ser. Advanced Textbooks in Control and Signal Processing. Springer London, 2010. [Online]. Available: https://books.google.de/books?id=jPCAFmE-logC

[32] K. Kronander and A. Billard, "Stability considerations for variable impedance control," *IEEE Transactions on Robotics*, vol. 32, no. 5, pp. 1298–1305, 2016.

[33] E. Shahriari, S. A. B. Birjandi, and S. Haddadin, "Passivity-based adaptive force-impedance control for modular multi-manual object manipulation," *IEEE Robotics Autom. Lett.*, vol. 7, no. 2, pp. 2194–2201, 2022. [Online]. Available: https://doi.org/10.1109/LRA.2022.3142903

[34] M. Simonič, R. Pahič, T. Gašpar, S. Abdolshah, S. Haddadin, M. G. Catalano, F. Wörgötter, and A. Ude, "Modular ros-based software architecture for reconfigurable, industry 4.0 compatible robotic work-cells," in *2021 20th International Conference on Advanced Robotics (ICAR)*, Dec 2021, pp. 44–51.

[35] S. Hjorth, E. Lamon, D. Chrysostomou, and A. Ajoudani, "Design of an energy-aware cartesian impedance controller for collaborative disassembly," in *2023 IEEE International Conference on Robotics and Automation (ICRA)*, May 2023, pp. 7483–7489.

[36] R. J. Kirschner, A. Kurdas, K. Karacan, P. Junge, S. Birjandi, N. Mansfeld, S. Abdolshah, and S. Haddadin, "Towards a reference framework for tactile robot performance and safety benchmarking," in *2021 IEEE/RSJ International Conference on Intelligent Robots and Systems (IROS)*. IEEE, pp. 4290–4297.